Journal of Hematology & Oncology

CORRESPONDENCE

Open Access

Identification of restrictive molecules involved in oncolytic virotherapy using genome-wide CRISPR screening

Yiye Zhong[1†], Huangying Le[1†], Xue Zhang[1†], Yao Dai[1], Fang Guo[1], Xiaojuan Ran[2], Guohong Hu[3], Qi Xie[2], Dawei Wang[4*] and Yujia Cai[1*]

Abstract

Oncolytic viruses (OVs) offer a novel approach to treat solid tumors; however, their efficacy is frequently suboptimal due to various limiting factors. To address this challenge, we engineered an OV containing targets for neuron-specific *microRNA-124* and *Granulocyte-macrophage colony-stimulating factor* (*GM-CSF*), significantly enhancing its neuronal safety while minimally compromising its replication capacity. Moreover, we identified PARP1 as an HSV-1 replication restriction factor using genome-wide CRISPR screening. In models of glioblastoma (GBM) and triple-negative breast cancer (TNBC), we showed that the combination of OV and a PARP inhibitor (PARPi) exhibited superior efficacy compared to either monotherapy. Additionally, single-cell RNA sequencing (scRNA-seq) revealed that this combination therapy sensitized TNBC to immune checkpoint blockade, and the incorporation of an immune checkpoint inhibitor (ICI) further increased the survival rate of tumor-bearing mice. The combination of PARPi and ICI synergistically enhanced the ability of OV to establish durable tumor-specific immune responses. Our study effectively overcomes the inherent limitations of OV therapy, providing valuable insights for the clinical treatment of TNBC, GBM, and other malignancies.

Keywords Oncolytic virus, PARP1, PD-1, Combination therapy, CRISPR screening

To the editor

OVs are natural or engineered viruses that selectively replicate within tumors [1]. However, the insufficient replication of OVs inside tumors remains a major obstacle, impeding their efficacy [2–4]. Hence, identifying the molecules that are targetable while replicating restrictive represents a viable strategy [5]. Herein, we developed a neuron-detargeted OV from herpes simplex virus 1 (HSV-1), and found its efficacy-restricting factors in viral replication and immune checkpoint pathways. Additionally, we designed an effective antitumor regimen by precisely combining OV, PARPi, and a programmed cell death protein 1 (PD-1) inhibitor, significantly extending the survival of mice in TNBC, GBM, and melanoma models, potentially supporting direct clinical translation.

†Yiye Zhong, Huangying Le and Xue Zhang contributed equally to this work.

*Correspondence:
Dawei Wang
wangdawei@shsmu.edu.cn
Yujia Cai
yujia.cai@sjtu.edu.cn
[1]Key Laboratory of Systems Biomedicine (Ministry of Education), Shanghai Center for Systems Biomedicine, Shanghai Jiao Tong University, Shanghai 200240, China
[2]School of Life Sciences, Westlake University, Hangzhou 310024, China
[3]CAS Key Laboratory of Tissue Microenvironment and Tumor, Shanghai Institute of Nutrition and Health, University of Chinese Academy of Sciences, Chinese Academy of Sciences, Shanghai 200031, China
[4]State Key Laboratory of Medical Genomics, National Research Center for Translational Medicine at Shanghai, Ruijin Hospital Affiliated to Shanghai Jiao Tong University School of Medicine, Shanghai 200025, China

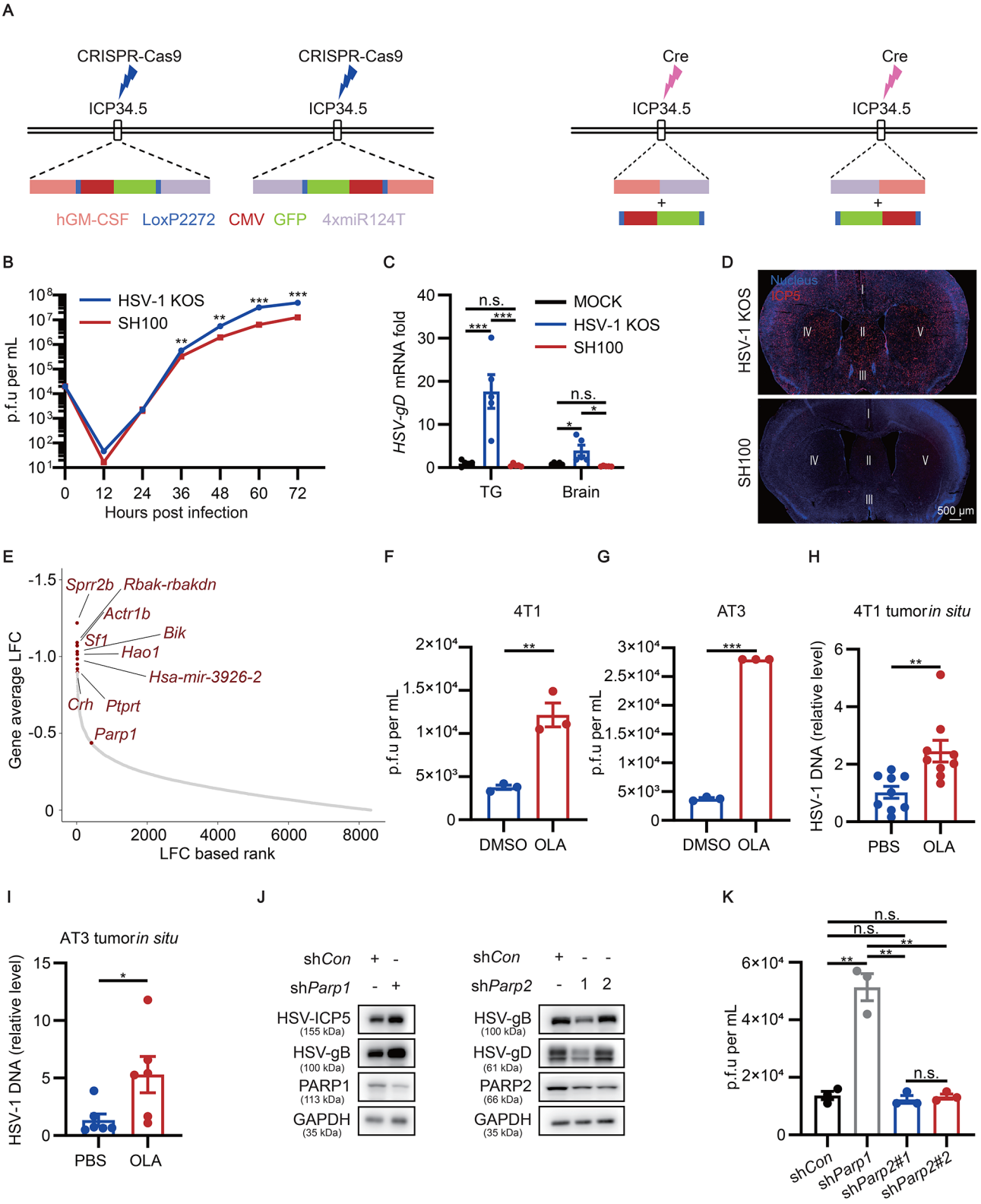

Fig. 1 (See legend on next page.)

(See figure on previous page.)

Fig. 1 Construction of a neuron-detargeted recombinant oncolytic HSV-1 and identification of its restriction factor PARP1. **A** Schematic illustration for the mechanism of constructing SH100. Donor sequence containing hGM-CSF, GFP and miR124T was inserted in both copies of the *ICP34.5* gene, which was facilitated by CRISPR. The intermediate product SH100-GFP (left) was treated with Cre to remove the GFP cassette to acquire SH100 (right). **B** Comparing replication of HSV-1 KOS and the isolated SH100 strain on Vero cells with one-step growth curve. MOI = 0.05. $n = 3$ per each time point. **C, D** Analysis of SH100 replication in neurons. After cornea infection of HSV-1 KOS and SH100 in the mice (7 dpi in Figs. 1C and 9 dpi in Fig. 1D), viral mRNA was detected by RT-qPCR (**C**), and the virus distribution in the brain was detected by immunofluorescence (**D**). $n = 5$ mice per group. ICP5 was indicated by red, DAPI was indicated by blue. **E** Average MAGeCK analysis for candidate restriction factors from genome-scale CRISPR screening. Top-ranked candidates were labelled. **F, G** 4T1 and AT3 cells were treated with 100 μM OLA for 12 h and infected with HSV-1 K26GFP (MOI = 0.8) for an additional 24 h ($n = 3$), followed plaque assay. **H, I** Mice received OLA or PBS intraperitoneal injection (i.p.) for 3 days, followed by intra-tumor injection (i.t.) of SH100 (5×10^7 PFU per mouse). After 2 days, tumors were collected and virus load was detected by qPCR of HSV-1 genomic DNA in 4T1 tumor model (**H**) ($n = 9$ mice per group) and AT3 tumor model (**I**) ($n = 6$ mice per group). **J, K** The impact of different shRNA on HSV replication. 4T1 cell lines were produced by transducing of shRNA-encoding lentiviral vectors and then infected with HSV-1 K26GFP (MOI = 0.8) for 24 h ($n = 3$), followed by Western blot (**J**) and plaque assay (**K**). *P* values were obtained by unpaired two-tailed *t* test (**B, C, F, G, H, I** and **K**). n.s., non-significant; $^{*}P < 0.05$, $^{**}P < 0.01$, $^{***}P < 0.001$. Data presented as the means ± SEM

We engineered SH100 by treating HSV-1 ICP34.5 under the control of *microRNA-124* which specifically expresses in neurons but is often silenced in tumors (Fig. 1A; Additional file 1: Fig. S2A) [6, 7]. One-step growth curves showed that SH100 proliferated as the wild-type virus (HSV-1 KOS) (Fig. 1B). Next, we evaluated the function of GM-CSF inserted in the SH100 and confirmed that SH100 expressed GM-CSF potently in different cell lines (Additional file 1: Fig. S2B-I). Notably, compared to its parent virus, the safety of SH100 greatly improved as indicated by the minimum presence in the trigeminal ganglia (TG) and brain (Fig. 1C, D; Additional file 1: Fig. S3). In contrast, its oncolytic activity was significantly enhanced in various cell types (Additional file 1: Fig. S4 A-H).

Using genome-wide CRISPR screening, we found poly (ADP-ribose) polymerase 1 (*Parp1*) which plays a vital role in DNA repair pathways and NAD^+ metabolism was among the top candidates (Fig. 1E; Additional file 1: Fig. S5A; Additional file 2: Table S1) [8, 9]. Since PARP1 is the only target with clinically available small molecules, we focused on PARP1 in subsequent studies. We pretreated 4T1 and AT3 cells, respectively, with olaparib (OLA), an inhibitor of PARP1/PARP2, before HSV-1 infection, and found that OLA significantly enhanced the viral replication (Fig. 1F, G; Additional file 1: Fig. S5B-F). Additionally, we confirmed the same observation with additional tumor cell lines in vitro and tumor models in vivo (Fig. 1H, I; Additional file 1: Fig. S5G-L). Extra studies demonstrated that knocking down PARP1 but not PARP2 boosted viral replication (Fig. 1J, K).

Next, we evaluated the synergistic antitumor effect of SH100 and OLA using a 4T1 TNBC lung metastasis model (Fig. 2A). Remarkably, the dual therapy exhibited a significantly reduced lung metastasis compared to SH100 alone, without affecting the body weight of the mice (Fig. 2B-D). We also demonstrated this synergistic effect in a GL261n-1 GBM model (Additional file 1: Fig. S6A-C). In addition, we examined the innate immune responses within primary tumors and found that intratumor injection of SH100 triggered the innate immune sensing, without detecting a significant difference to the SH100 + OLA group. (Additional file 1: Fig. S6D-I).

We then used scRNA-seq to analyze the status of T cells in 4T1 lung metastases models (Additional file 1: Fig. S7A-D). We found multiple immune checkpoint genes were upregulated in $CD4^+$Treg after dual therapy (Fig. 2E). Therefore, we supplemented the dual therapy with a PD-1 inhibitor. Indeed, we found triple therapy could further reduce lung metastases compared to dual therapy (Additional file 1: Fig. S8A, B). Additionally, we found increased lymphocyte infiltration, increased $CD8^+$ $PD\text{-}1^+$ T cells, and upregulation of immunosuppressive genes associated with M2-like macrophages in primary tumors (Additional file 1: Fig. S8, S9). As lung metastasis was still detected in nearly all mice, we reasoned it was due to delayed PD-1 antibody administration. Therefore, we optimized the regimen by injecting PD-1 antibodies only one day instead of five days after SH100 administration and evaluated efficacy in 4T1 and AT3 TNBC models, respectively (Fig. 2F; Additional file 1: Fig. S10A) [10]. The dual and triple regimens significantly suppressed primary tumor growth and alleviated lung metastasis in the AT3 model without significant toxicity (Fig. 2G-I; Additional file 1: Fig. S10B, C). However, the triple therapy showed the highest survival rates in both 4T1 and AT3 models, compared to dual therapy and the PD-1 inhibitor (Fig. 2J; Additional file 1: Fig. S10D), which was also validated in the B16F10n-1 melanoma model (Additional file 1: Fig. S10E-H).

To investigate tumor-specific immunological memory, we performed rechallenge study and found nearly all mice in combination groups were tumor-free except one with weak signals (Fig. 2K, L). IFN-γ enzyme-linked immunospot (ELISPOT) and cytometry by time of flight (CyTOF) analysis indicated that the combination therapy established long-term and systematic tumor-specific immunological memory (Fig. 2M; Additional file 1: Fig. S11-S12).

In summary, we developed a microRNA-regulated OV and found a triple combination therapy that efficiently overcame multiple constraints and significantly enhanced the antitumor effects. Our study may enhance

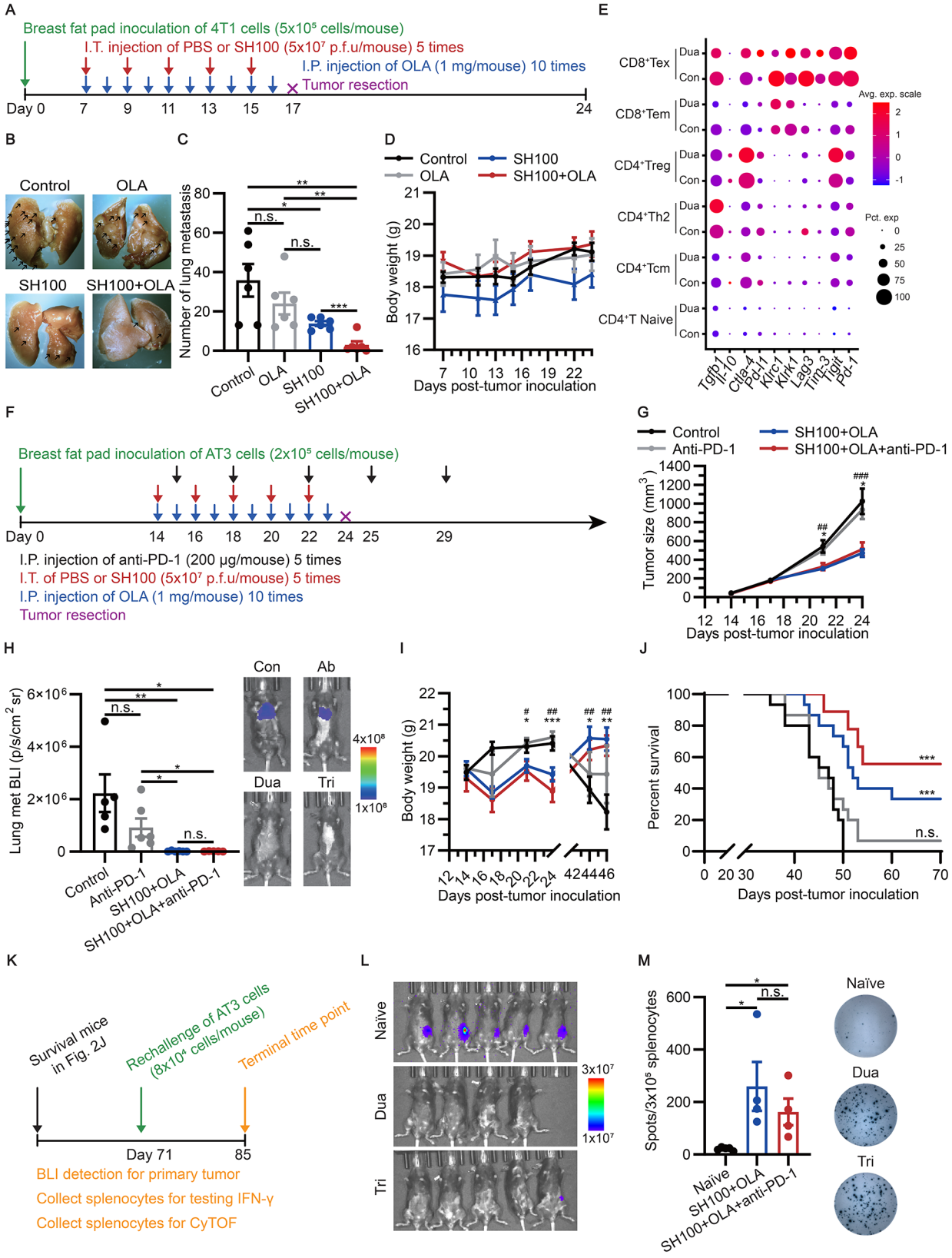

Fig. 2 (See legend on next page.)

(See figure on previous page.)

Fig. 2 Combination therapy blocked metastasis of TNBC and extended mice survival. **A** Illustration of optimized protocol for dual therapy in 4T1 tumors. **B** Representative images showing lung metastasis. **C** Statistical analysis of the number of lung metastasis. **D** The body weight of BALB/c mice bearing 4T1 tumors upon different treatments ($n=6$ mice per group). **E** Dot plot showed the expression levels of immune suppressive genes in different subtypes of T cells in the lung metastases of 4T1 models, where dot size and color represent percentage of gene expression (pct. exp) and the averaged scaled expression (avg. exp. scale) value, respectively. **F** Illustration of optimized protocol for triple therapy in AT3 tumors. **G-J** Evaluation the efficacy of optimized triple therapy in AT3 tumors. Tumor growth curves (**G**); lung BLI (**H**) (43 days post tumor inoculation); body weight (**I**); Kaplan-Meier survival curves of C57BL/6J mice bearing AT3 tumors (**J**). (**G, I** and **J**) Control, $n=15$, Anti-PD-1, $n=15$, SH100 + OLA, $n=15$, SH100 + OLA + anti-PD-1, $n=9$. (**H**) Control, $n=5$, Anti-PD-1, $n=6$, SH100 + OLA, $n=6$, SH100 + OLA + anti-PD-1, $n=6$. In (**G** and **I**), the symbol "*" denotes the difference between Control and SH100 + OLA + anti-PD-1. The symbol "#" denotes the difference between Control and SH100 + OLA. **K** Rechallenge scheme for survived mice in AT3 tumors. **L** Whole-body BLI analysis of tumor burden 14 days after AT3 cells reinoculation. **M** Interferon-γ (IFN-γ) ELISPOT analysis of splenocytes harvested 14 days after AT3 reinoculation. *P* values were obtained by unpaired two-tailed *t* test (**C, G, H, I** and **M**), n.s., non-significant, $^{*,\#}P<0.05$; $^{**,\#\#}P<0.01$; $^{***,\#\#\#}P<0.001$, or Mantel-Cox test (**J**), n.s., non-significant, $^{***}P<0.001$. Data were shown as the means ± SEM

the clinical efficacy of oncolytic therapy, providing better clinical translation for cancer patients.

Abbreviations

OV	Oncolytic virus
GM-CSF	Granulocyte-macrophage colony-stimulating factor
GBM	Glioblastoma
TNBC	Triple-negative breast cancer
PARPi	PARP inhibitor
scRNA-seq	Single-cell RNA sequencing
ICI	Immune checkpoint inhibitor
HSV-1	Herpes simplex virus 1
PD-1	Programmed cell death protein 1
TG	Trigeminal ganglia
PARP1	Poly (ADP-ribose) polymerase 1
OLA	Olaparib
ELISPOT	Enzyme-linked immunospot
CyTOF	Cytometry by time of flight

Supplementary Information

The online version contains supplementary material available at https://doi.org/10.1186/s13045-024-01554-5.

Supplementary Material 1

Supplementary Material 2

Supplementary Material 3

Supplementary Material 4

Supplementary Material 5

Supplementary Material 6

Acknowledgements
We thank Soren Riis Paludan at Aarhus University, Denmark, for the experimental materials and insightful discussion. We also thank Di Yin at Stanford University for helping with OV construction at the beginning of the project.

Author contributions
Y.C. conceived the study and designed the experiments; Y.Z., D.W., H.L. X.Z., Y.D., and X.R. performed the experiments or analysis; all the authors analyzed the data; Y.Z. and Y.C. wrote the manuscript with the help from all the authors.

Funding
Y.C. is supported by the National Natural Science Foundation of China (no. 31971364; 32370148), the National Key R&D Program of China (no. 2022YFC3400205), the Science and Technology Innovation Action Plan of Shanghai (24Z510200306), and the Key Forward-Looking Fund from Shanghai Jiao Tong University (no. AF4150049). D.W. is supported by Fundamental Research Funds for the Central Universities (no. YG2024QNB02), and the Guangci Distinguished Young Scholars Training Program (no. GCQN-2019-B17) and the Key-Research Fund from State Key Laboratory of Medical Genomics (no. 2022-13-2). X.Z. is supported by the National Natural Science Foundation of China (no. 82003781), Yangfan project from the Science and Technology Commission of Shanghai Municipality (no. 20YF1421900), and the Start-up Fund by Shanghai Jiao Tong University (no. 20X100040058).

Data availability
Single-cell RNA sequencing and Bulk RNA-sequencing datasets generated in this study are available on the GEO database under the accession numbers GSE207977 and GSE201760, respectively. Materials generated in this study are available upon request.

Declarations

Ethical approval and consent to participate
All animal-related experiments were performed under the guidelines of the Institutional Animal Care and Use Committee (IACUC) of the Shanghai Jiao Tong University with approval from the Animal Ethics Committee. When the tumor size reaches 1500 mm^3, the animals were euthanized. The maximal tumoral size did not exceed 1500 mm^3.

Consent for publication
Not applicable.

Competing interests
Y.C. is a co-founder and advisor of BDGENE Therapeutics. The other authors declare no competing interests. Y.C. filed a patent application (CN202111233544.9) related to this work.

Received: 30 January 2024 / Accepted: 6 May 2024
Published online: 23 May 2024

References

1. Aghi M, Martuza RL. Oncolytic viral therapies - the clinical experience. Oncogene. 2005;24(52):7802–16.
2. Raja J, Ludwig JM, Gettinger SN, Schalper KA, Kim HS. Oncolytic virus immunotherapy: future prospects for oncology. J Immunother Cancer. 2018;6(1):140.
3. Nemunaitis J, Senzer N, Sarmiento S, Zhang YA, Arzaga R, Sands B, et al. A phase i trial of intravenous infusion of onyx-015 and enbrel in solid tumor patients. Cancer Gene Ther. 2007;14(11):885–93.
4. Kirn D. Clinical research results with dl1520 (onyx-015), a replication-selective adenovirus for the treatment of cancer: what have we learned? Gene Ther. 2001;8(2):89–98.
5. Quillien L, Top S, Kappler-Gratias S, Redoute A, Dusetti N, Quentin-Froignant C, et al. A novel imaging approach for single-cell real-time analysis of oncolytic virus replication and efficacy in cancer cells. Hum Gene Ther. 2021;32(3–4):166–77.
6. Jia X, Wang X, Guo X, Ji J, Lou G, Zhao J, et al. Microrna-124: an emerging therapeutic target in cancer. Cancer Med. 2019;8(12):5638–50.
7. Sun Y, Luo ZM, Guo XM, Su DF, Liu X. An updated role of microrna-124 in central nervous system disorders: a review. Front Cell Neurosci. 2015;9:193.
8. Zada D, Sela Y, Matosevich N, Monsonego A, Lerer-Goldshtein T, Nir Y, et al. Parp1 promotes sleep, which enhances dna repair in neurons. Mol Cell. 2021;81(24):4979–93.

9. Alemasova EE, Lavrik OI. Poly(adp-ribosyl)ation by parp1: reaction mechanism and regulatory proteins. Nucleic Acids Res. 2019;47(8):3811–27.
10. Xiao Y, Cong M, Li J, He D, Wu Q, Tian P, et al. Cathepsin c promotes breast cancer lung metastasis by modulating neutrophil infiltration and neutrophil extracellular trap formation. Cancer Cell. 2021;39(3):423–37.

Publisher's Note